PCCP

Accepted Manuscript

ROYAL SOCIETY OF CHEMISTRY

www.rsc.org/pccp

Journal Name

RSCPublishing

ARTICLE

Features of chemical bonds based on the overlap polarizabilities: diatomics and solid-state systems with the frozen-density embedding approach

Renaldo T. Moura Jr*, Gian C. S. Duarte, Thiago E. da Silva, Oscar L. Malta, Ricardo L. Longo*

'Cite this: DOI: 10.1039/xoxxoooooox

Received ooth January 2012,
Accepted ooth January 2012

DOI: 10.1039/xoxxoooooox

www.rsc.org/

The chemical bond overlap properties were obtained for alkali halides NaY (Y = F, Cl, Br), alkaline-earth chalcogenides MX (M = Ca, Mg and X = O, S, Se) and alkali and alkali-earth metals (Li, Na, and Mg) in diatomic and solid-state systems using an embedding approach based on the Frozen Density Functional Theory to simulate the crystalline effects. The computational protocol established provides errors for bond distances smaller than 1%. The results indicate that larger chemical bond covalency lead to larger absorption or scattering by the overlap region. The ionic specific valence and overlap polarizability are closely related to the valence orbitals compactness measured by the sum of Mulliken electronegativities. The embedding approach used in this work makes it possible to quantify the effects of the crystalline environment on the chemical bond overlap properties. In solid-state, the bond overlap charges are less polarizable, in cases of well-known ionic systems (provided by electronegativity differences), leading to smaller chemical bond covalency in solids than in diatomics. The spectroscopic properties of the polarizability of the electron density in the overlap region of a chemical bond could be measured in the 1–20 eV spectral region and could be used to characterize some bands in several spectra whose assignments are ambiguous or not available.

1 Introduction

The properties of molecular and solid-state compounds depend on the type and nature of their atomic constituents, how these atoms interact with each other and their spatial structure. In particular, the knowledge of the interaction between the atoms has motivated the development of the concept of chemical bond, which is central to the understanding of chemistry and for describing many chemical-based processes. At the dawn of the 20th century, Lewis introduced the concept of covalent bond into chemistry by defining a covalent bond as a pair of electrons being shared by two atoms.[1] To distinguish from the concept of valence used in the valence theory at that time, the term covalency was introduced by Lagmuir[2] and defined as the number of pairs of electrons that a given atom shares with its neighbours.

The first treatment of the covalent chemical bond in H_2 molecule using quantum mechanics was performed by Heitler and London in 1927.[3, 4] Pauling was the first to propose a quantitative measurement of the covalency and ionicity concepts based on the electronegativity differences of the atoms involved in the bond.

In solid-state chemistry, the type of atom and the chemical bond play an important role at characterizing the type of solid (metallic, ionic, covalent, molecular, etc.) and its properties. Discussions about the nature of the chemical bond in crystals were based, for instance, on thermochemical (Pauling)[5], valence bond (Coulson)[6] and spectroscopic (Phillips)[7] theories. Indeed, Pauling was able to correlate the electronegativity concept (and so the ionicity) to thermochemical data, while Coulson formulated the concepts of electronegativity and ionicity in the language of molecular orbitals by using the definition of electronegativity given by Mulliken. The so-called spectroscopic theory for the chemical bond in a crystal was based on a model Hamiltonian and used a set of parameters obtained from spectroscopic data,[7] which provided a relationship between the ionicity and the energy gap in crystals. Noteworthy that relationships were established between the covalency (and ionicity) concept in chemical bonds in solids and structural, thermochemical and optical properties, for instance, *i*) binary compounds with large electronegative differences tend to form rock salt structures; *ii*) more ionic compounds usually have larger heats of formation; and *iii*)

more covalent compounds tend to have lower bandgap energies. It is thus important to have accurate and reliable tools for quantifying the covalency in solid and molecular materials that can reveal aspects about the electron sharing in chemical bond and its consequences for the properties in the solid-state.

The concepts of chemical bond overlap polarizability (α_{OP}) and ionic specific valence (ISV) were introduced during studies related to ligand field theory applied to lanthanide compounds[8] and led to relevant conclusions on the interpretation of the non-spherical ligand field interactions in terms of covalency.[8, 9] As a result, a covalency scale and a description of the ligand field in these compounds were created,[9] so that some empirical parameters in the Simple Overlap Model[10] could be associated, for instance, with the ISVs of the ligating atoms.

The α_{OP} and ISV concepts were also explored in the case of diatomic molecules, so a new covalency scale, analytically quantifiable in terms of the α_{OP}, was established[11, 12] in excellent agreement with Pauling's scale[11]. More recently, a proposal in which the overlap region was regarded as a localized *plasmon-like* charge distribution (chemical bond overlap *plasmon-like* – CBOP), characterized by the overlap polarizability, has raised the possibility of absorption and inelastic scattering of radiation by the overlap region, above the first ionization threshold.[12] An interesting aspect is that, formally, oscillation modes corresponding to σ and π bonds can be distinguished by these processes, on the grounds of their quite distinct electron densities as, for instance, in the carbon monoxide molecule. In addition, the theoretical possibility of detecting the CBOP in diatomic molecules by electron inelastic scattering was explored,[13, 14] including the quadrupole nature of the CBOP energy-loss cross section.[13]

Our most recent studies showed that the CBOP may be a promising tool for quantifying covalency in solid-state materials,[14] where the CBOP properties for solid-state alkali halides were obtained with a point-charge scheme for mimicking the crystalline environment. It was shown that the CBOP energies for the alkali halide crystals are quite close to experimental transition energies ambiguously assigned as excitons or surface plasmons. Thus indicating that the CBOP could be an alternative assignment to the observed structures and shoulders in the 5-15 eV region.[14] This computational approach[14] proved to be robust for ionic crystals, but was limited to those systems. Thus, for more covalent solids such as aluminum, silicon or tin oxides, this point-charge approach presented difficulties for convergence, for creating the appropriate clusters, and for stabilizing the O^{2-} species, which raised some questions about the quantitative aspects of the results.

Thus, a proper description of the crystalline environment around a chemical bond is conceptually and quantitatively important because it could aid at establishing relationships between macroscopic properties of materials and concepts associated with the overlap charge density. For example, a good correlation was already found between the non-linear index of refraction and the α_{OP}.[12] The main goal of the present contribution is to extend the concepts and the calculations of the chemical bond overlap properties to solid-state materials. An embedding approach based on the Frozen Density Functional Theory (FDFT) was successfully used to simulate the crystalline effects. The quantitative results provided, for instance, an alternative characterization of unassigned or ambiguously assigned bands in the electron energy-loss spectra of solid-state systems such as alkaline-earth chalcogenides and some alkali and alkali-earth metals, as well as, the effects of the crystalline environment into the chemical bonds by comparisons with the respective isolated diatomic system.

2 The concepts of overlap polarizability and ionic specific valence

The formulation of the chemical bond overlap polarizability and the ionic specific valence was presented elsewhere[11-14] and shall be only briefly reviewed.

Starting from the general quantum mechanical sum-over-states expression for the polarizability of a field-free molecule and expanding the monoelectronic molecular orbitals as a linear combination of atomic orbitals, the molecular polarizability can be approximated by[14]

$$\alpha \cong \frac{2e^2}{\Delta\varepsilon}\sum_{\xi}\sum_{\zeta}\left|\left\langle \xi\left|\vec{r}\right|\zeta\right\rangle\right|^2 F(\xi,\zeta) \qquad 2.1$$

where e is the elementary charge, $\Delta\varepsilon$ is an effective energy difference between the relevant states, and the summation runs over the valence sub-shells of atoms A and B. Thus, the diagonal one-center matrix elements lead to the atomic polarizabilities, namely,

$$\alpha_{X} = \frac{2e^2}{\Delta\varepsilon}\sum_{\xi\in X}\sum_{\zeta\in X}\left|\left\langle \xi_{X}\left|\vec{r}\right|\zeta_{X}\right\rangle\right|^2 F(\xi_{X},\zeta_{X}) \qquad 2.2$$

for X = A or B, and the off-diagonal two-center matrix elements lead to the overlap polarizabilities,

$$\alpha_{OP} = \frac{2e^2}{\Delta\varepsilon}\sum_{\xi\in A}\sum_{\zeta\in B}\left|\left\langle \xi_{A}\left|\vec{r}\right|\zeta_{B}\right\rangle\right|^2 F(\xi_{A},\zeta_{B}) \qquad 2.3$$

with $F(\xi_A,\zeta_B)$ being a function of the coefficients of the valence atomic orbitals entering in the compositions of the HOMO and LUMO. The homopolar dipole approximation[15] may be employed for the dipole matrix elements, $\left\langle \xi_{A}\left|\vec{r}\right|\zeta_{B}\right\rangle$, for typical values of bond distances and atomic orbitals that are not diffuse. The factor $F(\xi_A,\zeta_B)$ can be obtained from the contributions of the atomic orbitals to the molecular states, which can be determined by standard electronic structure methods, as long as, these molecular states are localized onto the A–B moiety.[11, 14] These contributions depend mainly upon the overlap between the atomic orbitals involved in the chemical bond. Thus, in order to have a general approach that is independent on the electronic structure method, a power series

expansion in terms of ρ^2, where ρ is the overlap integral, of the summation in Eq. 2.3 may be performed and truncated at the second term because $\rho^2 << 1$. As a result, the polarizability of the chemical bond is readily separated into a contribution from the interacting species A and B, and a contribution from the overlap region,[8, 11, 14]

$$\alpha \cong \alpha_A + \alpha_B + \alpha_{OP} \quad 2.4$$

with the polarizability of the overlap region expressed as,

$$\alpha_{OP} = \frac{e^2 R^2 \rho^2}{2\Delta\varepsilon} \quad 2.5$$

where R is the bond distance and ρ the overlap integral. Noteworthy that the $\Delta\varepsilon$ quantity in Eq. 2.5 is an excitation energy between states that are fully localized in the chemical bond and its determination becomes a challenge for polyatomic and solid-state systems.

The electron density confined in the overlap region or more simply the overlap charge, q, increases with the overlap volume and, therefore, with the polarizability of the overlap region, α_{OP}. However, this relationship is not linear and it involves the square of the charge through a force constant,[16] which was postulated to be the force constant, k, of the chemical bond, such that,

$$q^2 = k\alpha_{OP} \quad 2.6$$

On the other hand, the overlap charge (q) should be proportional to the overlap (ρ), that is,

$$q = pe\rho \quad 2.7$$

where p is a proportionality constant. If a polar chemical bond between A and B is pictured as being formed from an acid-base type reaction ($A^+ + B^-$), then the factor p may be expressed as the sum of contributions from both species, namely, p_c from A^+ and p_a from B^-. As a result, when using Eqs. 2.5 and 2.6 into Eq. 2.7, the ionic specific valences of A^+ (υ_c) and B^- (υ_a) were introduced.[8, 11, 14] These quantities may be interpreted as the capacity of the atomic species to donate electron density to the formation of the A–B bond, and thus, $\upsilon = \upsilon_c + \upsilon_a \approx 1$. This qualitative interpretation is connected with the electronegativities of the species involved in the chemical bond, where it is expected that species A^+ would be more electronegative and B^-. Noteworthy that the ionic specific valence (υ) is a general concept and readily applicable to polar bonds as well as for homonuclear bonds: $\upsilon_c = \upsilon_a \cong \frac{1}{2}$. Assuming that the proportionality constant p in Eq. 2.7 is the ionic specific valence (υ), it is found that

$$\upsilon = p = R\sqrt{\frac{k}{2\Delta\varepsilon}} \quad 2.8$$

Thus, the charge density confined in the overlap region becomes

$$q = \upsilon e\rho = e\rho R\sqrt{\frac{k}{2\Delta\varepsilon}} \quad 2.9$$

Because the cores of the A and B species attract this charge density and confine it in the overlap region, it may be expected that the overlap charge density would interact with fields (*e.g.* electromagnetic oscillating fields) and electron beams differently from the other charge densities in the system, such as that of the A and B cores or lone electron pairs. In fact, static electric fields would induce polarization of the charge density confined in the overlap region, which is described by the polarizability of the overlap region, α_{OP}. On the other hand, electromagnetic fields would induce oscillations of this confined overlap charge, whereas electron beams would be, for instance, scattered by it. In analogy with a picture discussed by Jackson[17] that described a charge density interacting with oscillating fields as *plasma*, this charge density confined in the overlap region was denoted previously as *plasmon-like*.[12-14] However, because plasmons are now more commonly employed in the description of collective oscillating modes of charge densities, especially, surface charges, there has been some confusion on this terminology. Thus, we shall refer to the charge density confined in the overlap region of a chemical bond simply as *overlap charge* or more specifically as chemical bond overlap charge. In addition, the properties of the overlap region in a chemical bond, such as charge density, polarizability (α_{OP}), mass, volume, etc., shall be denoted generically as chemical bond overlap properties.

In the following subsection, the theoretical framework for probing the overlap charge with photons (*e.g.*, absorption, excitation, inelastic scattering) and electrons (*e.g.*, energy-loss cross section) shall be briefly presented.[12-14]

3 Absorption, inelastic scattering and electron energy-loss by the chemical bond overlap charge

The overlap charge confined by the cores of A and B is described by a harmonic potential with force constant k, in order to be consistent with the proposed model and with the postulate in Eq. 2.6. By assigning an effective mass (m) to the overlap region, a semi-classical harmonic oscillator picture emerges that was used to calculate the absorption and Raman scattering processes by the overlap charge as depicted in Figure 1. The energy-loss cross section of an electron beam scattered by the overlap charge was also calculated.[12-14] The energy dissipation by the overlap charge shall occur almost entirely through non-radiative energy transfer channels, leading to bound-to-bound state transitions, dissociation, photoelectrons and heat production.

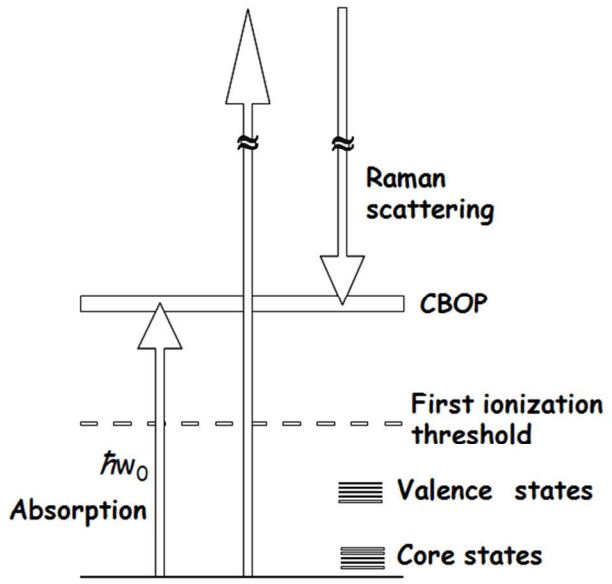

Figure 1. Schematic level diagram indicating the absorption and Raman scattering processes by the overlap electron density confined into a chemical bond.

This semi-classical oscillator having a mass of the overlap region given by,[12-14]

$$m = \upsilon\rho m_e \qquad 3.1$$

with m_e being the electron mass, has an fundamental angular frequency, ω_0, expressed as

$$\omega_0 = \sqrt{\frac{k}{m}} \qquad 3.2$$

with *k* being the bond force constant as assumed in Eq. 2.6. The corresponding characteristic energy (absorption) is

$$E_p = \hbar\omega_0 \qquad 3.3$$

The oscillator strength, *f*, associated with electromagnetic energy absorption for this characteristic energy is given by[12-14]

$$f = \frac{2m\omega_0}{3\hbar e^2}\mu^2 \qquad 3.4$$

where the transition electric dipole moment, μ, is given by the approximation employed in Eq. 2.3, namely,

$$\mu \cong \frac{1}{2}eR\rho \qquad 3.5$$

where *R*, *e* and ρ were already defined.

The dispersion relation of Kramers-Heisenberg for a semi-classical oscillator can be used to obtain the cross-section for the Raman scattering, σ_{Raman}, which in the high frequency regime is approximately given by[12-14]

$$\sigma_{Raman} = \frac{4\pi\omega\omega_s^3}{c^4}\left[\left(\frac{\Delta\varepsilon}{\hbar\omega}\right)^2\alpha_{OP}\right]^2 \qquad 3.6$$

where ω and $\omega_S = \omega - \omega_0$ are the angular frequencies of the incident and scattered photons, respectively, $\Delta\varepsilon$ is the excitation energy as used in the overlap polarizability, α_{OP}, in Eq. 2.5.

In the inelastic scattering process by the chemical bond overlap charge, an incident electron beam with wave vector $\vec{K}$ is scattered by the target and acquires a wave vector $\vec{K}'$. The total cross section in a scattering solid-angle can be expressed as[12, 13]

$$\sigma_{Loss} = \frac{2\pi^2}{3\hbar^2}\frac{e^4\upsilon^2\rho^4R^2m}{E_p}\int_{\theta_1}^{\theta_2} d\theta_q \frac{\cos^2\theta_q \sin\theta_q}{1-\cos\theta_q} \qquad 3.7$$

where $\vec{q} = \vec{K} - \vec{K}$ is the angle between the incident and scattered electron beam, and the aperture of the detection instrument defined by the difference $\theta_2 - \theta_1$ is assumed to be 3° to 5°.

4 Computational Models and Procedures

The theoretical framework describing the properties of the chemical bond based on overlap polarizabilities (α_{OP}) and overlap charges was employed and applied to solid-state systems such as alkali-earth chalcogenides MX (M = Ca, Mg and X = O, S, Se), alkali and alkali-earth metallic systems Li, Na and Mg. This selection was motivated by previous theoretical and computational results[10-12] showing relationships between the overlap polarizability (α_{OP}) and covalency. The data required to calculate the ionic specific valence (υ) the overlap polarizability (α_{OP}) and the overlap charge properties namely, *R*, ρ, $\Delta\varepsilon$ and *k* were obtained with an embedding approach to simulate the crystalline effects. From these quantities, some properties of the CBOC were calculated, such as, absorption wavelengths (λ_0) and their respective oscillator strengths (*f*), incident (λ) and scattered photon wavelengths (λ_s) and their respective scattering cross-sections (σ_{Raman} and σ_{Loss}), as well as the values of the overlap charge wavelengths (λ_p) and energies (E_p).

In order to maintain the localized nature of the overlap charge density model, the distances (*R*) and bond force constants (*k*) in the solid structures were calculated using a cluster model embedded into the crystalline environment, where a central cluster was treated self-consistently and the environment embedding clusters were treated as frozen densities. The overlap (ρ) between the valence orbitals of the MX pair was calculated at the equilibrium distance in the crystal structure using the following expression for the overlap, S_{ij}, between the valence orbitals in atoms A and B (see Supporting Information),

$$S_{ij} = \sum_k\sum_l (a_k b_l) O_{kl} \qquad 4.1$$

where a_k and b_l are the coefficients of the basis functions centered at atoms A and B, respectively, and O_{kl} is the overlap integral between the basis functions k and l used to describe the atomic valence subshells. Equation 4.1 makes it possible to take into account the embedding density effects self-consistently through the a_k and b_l coefficients.

For the calculation of the excitation energies ($\Delta\varepsilon$), this model is not appropriate because the electronic states could be delocalized over the self-consistent central cluster, thus violating one of the main assumptions of the overlap charge framework, namely, the diatomic-like behavior. Thus, a new model was created which included only the M–X pair as explicit atoms in the self-consistent part embedded into the crystalline frozen density (relaxed) environment. For implementing this model for the overlap charge density, the Frozen Density Functional Theory (FDFT)[18] formalism appears to be an appropriate choice because it can take into account the crystalline environment while keeping the bond of interest in a diatomic-like state. In this approach, the embedding of a self-consistent cluster or MX diatomic species into the crystalline environment was performed by the Frozen Density Embedding (FDE) implemented in ADF program[19] as briefly described in the following section.

4.1 The Frozen Density Embedding Approach

A simplified approach to treat chemical processes in solution was developed based on DFT (density functional theory).[18] This approach, denoted as frozen DFT (FDFT), consists in freezing the electron density of the solvent molecules, while solving the self-consistent problem for the solute Hamiltonian that includes the effective potential of the solvent molecules. The FDE theory was explained in literature[18] and only a brief introduction to allow explanations of the computational procedure and of the discussions of the calculated results. In an example of the FDFT simplification, an N-electron system is divided in two subsystems S_1 and S_2 with N_1 and $(N - N_1)$ electrons, respectively. Accordingly, the total electron density can written as

$$\rho(\vec{r}) = \rho_1(\vec{r}) + \rho_2(\vec{r}) \qquad 4.2$$

where $\rho_1(\vec{r})$ and $\rho_2(\vec{r})$ are the electron density of subsystems S_1 and S_2, respectively. If $\rho_2(\vec{r})$ satisfies the condition

$$\int \rho_2(\vec{r})\, d\vec{r} = N - N_1 \qquad 4.3$$

then, $\rho_1(\vec{r})$ is the density that minimizes the total energy of the system, $E[\rho(\vec{r})]$, and is expressed in terms of the Kohn-Sham orbitals as

$$\rho_1(\vec{r}) = 2\sum_{i=1}^{N_1/2} \varphi_i^* \varphi_i \qquad 4.4$$

In this procedure, it is possible to express the effective potential (V_{eff}) in the same way as in the original Kohn-Sham method. However, the kinetic energy cannot be written in the same way because the Kohn-Sham determinant of the overall system (subsystems S_1 and S_2) is not known. Thus, the FDFT formalism approximates the kinetic energy functional as a sum of the kinetic energies from the densities for $\rho_1(\vec{r})$ and $\rho_2(\vec{r})$ with a non-additive term correction T_S^{nad}. As a result, the Euler equation in the FDFT method for the two subsystems (S_1 being self-consistent and S_2 being frozen) is expressed as[12]

$$\mu' = V(\vec{r}) + \int \frac{\rho_2(\vec{r})}{|\vec{r} - \vec{r}'|} d\vec{r}' + \int \frac{\rho_1(\vec{r})}{|\vec{r} - \vec{r}'|} d\vec{r}' + V_{xc}(\vec{r}) + \frac{\delta T_s^{\text{nad}}[\rho_1, \rho_2]}{\delta \rho_1(\vec{r})} + \frac{\delta T_s[\rho(\vec{r})]}{\delta \rho(\vec{r})} \qquad 4.5$$

The solution of equation 4.5 can be obtained similarly to the original Kohn-Sham method by solving

$$\left[-\frac{1}{2}\nabla^2 + V_{\text{eff}}(\vec{r}) + \frac{\delta T_s^{\text{nad}}[\rho_1, \rho_2]}{\delta \rho_1(\vec{r})} \right] \varphi_i = \varepsilon_i \varphi_i \qquad i = 1,2,\ldots,N_1/2 \qquad 4.6$$

Equations 4.4, 4.5 and 4.6 form then a new scheme of self-consistent calculation analogous to the Kohn-Sham DFT method, although in FDFT simplification, part of the electron density (related to $(N - N_1)$ electrons) is frozen. Thus, instead of solving the N-electron problem, it is possible to solve the N_1-electron problem using the new effective potential $V_{\text{eff}}^{\#}$,

$$V_{\text{eff}}^{\#}(\vec{r}) = V_{\text{eff}}(\vec{r}) + \frac{\delta T_s^{\text{nad}}[\rho_1, \rho_2]}{\delta \rho_1(\vec{r})} \qquad 4.7$$

The FDFT approach was successfully employed in the description of several systems[20-23] and it is quite suitable for the CBOC model because by freezing the electronic density of the surrounding atoms, the orbitals shall be localized in the self-consistent portion of the system, however, the effects of the environment (e.g., crystalline effects) are taken into account.

4.2 Solid-State Embedding Scheme with the FDE scheme

Initially, the electron density of a selected isolated cluster, which may be a unit cell or not, is obtained self-consistently. Subsequently, this electron density is frozen and replicated around a central cluster to mimic the crystalline environment. In the replicated system, the electron density of the central cluster is obtained by the FDFT approach under the influence of the frozen densities of the neighboring clusters. The current implementation of the ADF program does not perform analytical gradient calculations using the FDE approach. Therefore, a code was developed to perform a geometry optimization of a single distance in the central cluster using a modified Brent method based on gradients.[24] In addition, this code can perform automatically the entire process, namely, generates the isolated cluster electron density, replicates the cluster in space, and builds the ADF input file for a FDE calculation. The scheme used to mimic the crystalline effects is depicted in Figure 2.

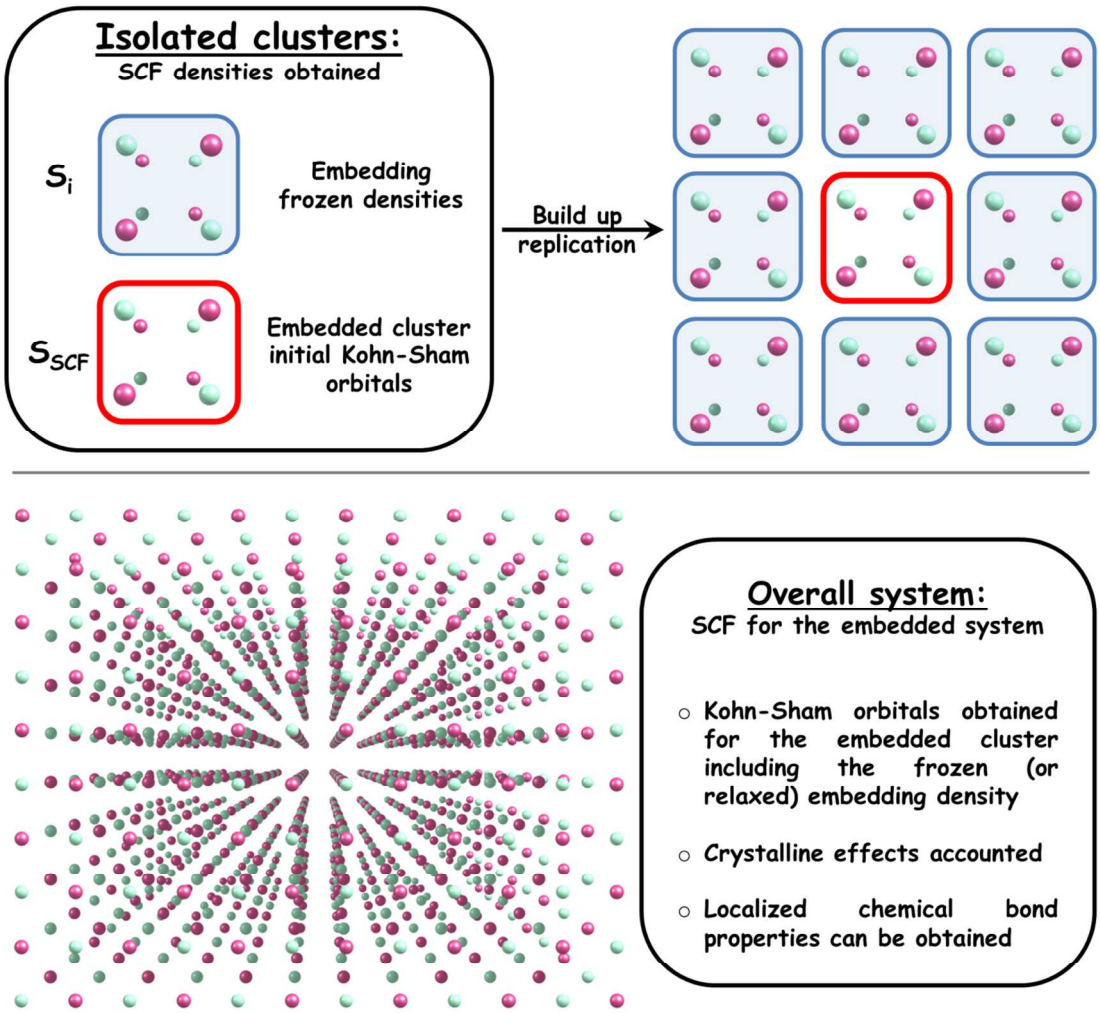

Figure 2. Schematic representation of the Frozen Density Embedding approach used in the calculation of the bond distance, bond force constants, bond excitation energy, and overlap integral for crystalline structures. S_i are clusters with frozen densities, S_{scf} is the cluster for which the Kohn-Sham orbitals will be obtained under the influence of crystalline effects.

Once the frozen and self-consistent subsystems (S_i and S_{SCF} in the Figure 2, respectively) are defined and the desired chemical bond is selected, the code provides the force constant (k), the excitation energy ($\Delta\varepsilon$), and the overlap (ρ) for the chemical bond.

Into the code was implemented the option to scan the bond distance of interest, so that the force constant can be calculated from a quadratic polynomial fit as $k = 2b_2$, with b_2 being its quadratic coefficient. It was also implemented into de the calculation of the numerical second derivative of the energy with respect to distance, thus allowing the direct estimate of the force constant that can be used to check the value obtained by the polynomial fitting procedure.

The calculation of the excitation energy is performed by freezing the entire self-consistent cluster (S_{SCF} in the Figure 2), except for the two atoms involved in the desired chemical bond. In this case, the frozen density of this nearest neighbor is relaxed in a freeze-and-thaw calculation. In this process, the embedded subsystem (the bonded atom pair on S_{SCF} in the Figure 2) is frozen, while this fragment is thawed. This process is repeated until convergence is reached. By relaxing the frozen fragments, it is possible to improve the environment density by taking into account the polarization of the environment by the embedded system.[25]

The overlap (ρ) between the valence atomic orbitals of the atoms forming the chemical bond of interest was calculated from the overlap integrals in the selected basis set and their corresponding SCF coefficients by using equation 4.1.

All calculations employed the BLYP functional with DZ, DZP, TZP e TZ2P Slater-type basis sets for the SCF. The excitation energy calculations used the TDDFT approach with the same functional and basis set. The non-additive kinetic energy term of the embedding part was described by the recommended[18] PW91K functional.[26] All calculations were performed with the ADF program[19] using its default criteria and increasing the numerical integration criteria to INTEGRATION 10.0 or 12.0.

The calculations of the isolated diatomic species were also perfomed with the ADF program[19] using the same functional (BLYP) and basis sets at the calculated equilibrium bond distance.

5 Results and Discussion

Because this is the first time that the FDE approach is applied in the description of the crystalline environment, it needs to be properly validated and a computational protocol established, which involves the selection of the basis set and the choice of the replication scheme. The basis sets tested were listed in the previous section and the following replications: 3×3×3, 5×5×5 and 6×5×5 were tried. In the first two replications, the frozen and the self-consistent clusters are former by eight atoms, whereas in the 6×5×5 replication, the clusters are formed by sixteen atoms. Figure 3 depicts the energy curves for each replication scheme and basis set for the NaCl system.

For the 3×3×3, 5×5×5 replications, the calculated energy minimum is *ca*. 2.6 Å for all basis sets. Comparison with the experimental distance for Na–Cl bond (2.81 Å), suggests that these replication schemes to freeze the density of the neighbor cells are not adequate to provide a proper description of the crystalline effects. It may be observed that the energy profile in Figure 3a has a cusp at distances near the experimental value. This may be a consequence of the fact that the atoms directly bonded to the analyzed chemical bond have their densities frozen. Thus, to correct these flaws of these embedding schemes a larger self-consistent cluster was employed. Indeed, with the 6×5×5 replication scheme, the energy curves for the tested basis sets show a minimum at distances very close the experimental one, as can be observed in Figure 3b. As a result, the bond parameters and the overlap density properties were calculated with the 6×5×5 replication and the TZ2P basis set for three systems (NaF, NaCl, NaBr) whose properties had already been calculated[14] with a point charge embedding approach. For these systems, the equilibrium distance and its gradient and Hessian (to provide the force constant), the excitation energy and the overlap were calculated and are presented in Table S1 (Supporting Information). Noteworthy that the errors between the calculated and experimental bond distances are smaller than 1%, indicating that this frozen density embedding with a 6×5×5 replication and a TZ2P basis set is an accurate protocol to mimic the crystalline effects for a local chemical bond. In addition, there is a complete agreement between the force constants calculated by the Hessian (second derivative of the energy with respect to the distance) and the quadratic polynomial fit of the energy with respect to the distance.

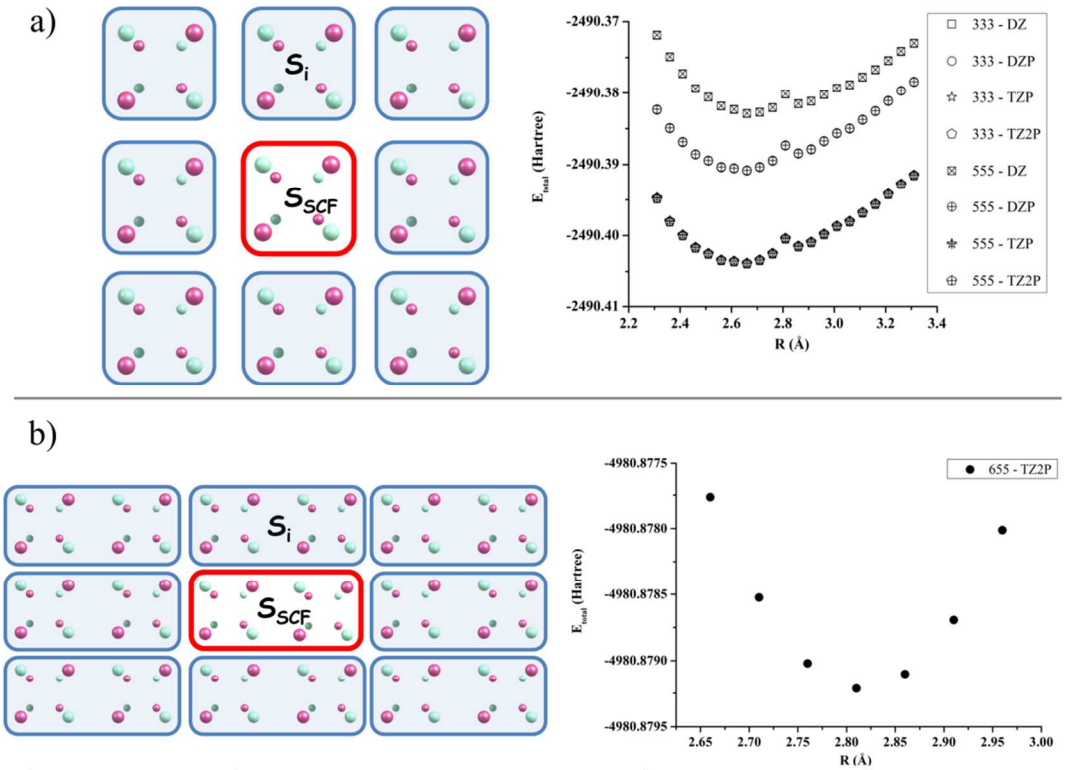

Figure 3. Energy profiles obtained with BLYP functional and DZ, DZP, TZP and TZ2P basis sets for the test system NaCl. a) For the replications 3×3×3 and 5×5×5 in which the frozen and the SCF clusters have eight atoms. b) For a replication 6×5×5 in which the frozen and the SCF clusters (with sixteen atoms) was calculated with BLYP/TZ2P.

A second test performed was the calculation of the force constant using a complete reference system to ascertain the consistence of the embedding results. Namely, the reference consisted of replications $n \times n \times n$ with n = 3, 4, 5, and 6 for a Li

crystalline system, where the energy was calculated for different distances between two central atoms. Considering symmetry in calculations, at the equilibrium distance, the SCF convergence is usually achieved, while for other distances, the change in point group of the whole system introduces a drastic convergence problem. Only for the smallest replication 3×3×3 we were able to perform the calculations without symmetry that provided a force constant of 0.32×10^5 dyn cm^{-1} and an equilibrium distance of 2.9 Å. Given the size of the replication and the relative error to the experimental bond distance, the results for the force constant with and without embedding are compatible and comparable. It is important to emphasize that the application of full periodic calculations (such as plane waves) for the overlap polarizability model requires a very large unit cell (supercell) to ensure that there are no intracell interactions between the underlying quantities. In addition, a full periodic calculation would be unable to provide the underlying properties of the overlap except the force constant. Noteworthy that the small errors calculated for the bond distances do suggest that this proposed embedding approach is quite reliable.

From the underlying quantities (R, ρ, k, and Δε) characterizing the overlap density presented in Tables S1-S3 (Supporting Information), its properties related to covalency (polarizability, α_{OP} and ionic specific valence, υ) and to spectroscopy (absorption wavelength and oscillator strength, scattered wavelength and Raman cross-section, electron energy-loss cross-section, characteristic energy) were calculated and are presented in Table 1. Noteworthy that these properties for alkali halides (NaF, NaCl, NaBr) follow the same trend already observed and discussed for these systems using a modified point-charge embedding scheme,[14] thus indicating that the present frozen density embedding approach are consistent with preview results. This validation indicates that the replication 6×5×5 scheme with the TZ2P basis set is an appropriate computational protocol to explore the overlap density properties in solid-state systems and was employed for the remaining systems.

The accuracy and robustness of the computational methodology developed may be ascertained by the small errors (< 3% in Tables S1 and S2, except for Na metal) related to the calculated equilibrium bond distances in wide range of crystalline solid-state structures such as NaY (Y = F, Cl, Br), MX (M = Ca, Mg and X = O, S, Se) and Li, Na, and Mg metals.

Regarding the parameters of the chemical bonds, a systematic trend was observed for a fixed chalcogenide. For instance, the force constant decreases when going from Mg to Ca in the MX (X = O, S, Se) diatomic systems but increases in the crystal series. Furthermore, the overlap integrals follow the same trend in both diatomic and crystalline systems (Tables S2 and S3). It has been established for diatomic molecules that as the percent of the ionic contribution to the chemical bond increases, the force constant also becomes larger.[27]

Table 1. Spectroscopic and covalency properties of the overlap charge density for alkali halide, alkali-earth chalcogenide and metal crystal structures. Absorption wavelength λ_0 (nm) and its respective oscillator strength, f, Scattered λ_S photon wavelength (nm) and its respective scattering (Raman) cross-section σ_{Raman} (10^{-26} cm^2). Electron energy-loss cross-section σ_{Loss} (10^{-22} cm^2). Overlap charge characteristic energy E_p (eV). Overlap polarizability α_{op} (Å^3) and ionic specific valence υ.

Crystal	λ_0	f	λ_S	σ_{Raman}	σ_{Loss}	E_p	α_{op}	υ
NaF	792	0.004	883	0.0201	0.0044	15.5	0.068	1.239
NaCl	1044	0.005	696	0.0263	0.0075	11.8	0.136	1.551
NaBr	1032	0.002	701	0.0097	0.0020	11.9	0.088	1.366
CaO	1582	0.318	567	5.9728	6.0752	7.78	2.389	2.708
CaS	2487	0.617	502	32.936	23.134	4.95	7.353	2.548
CaSe	2224	1.019	514	50.184	43.917	5.54	7.568	3.192
MgO	1724	0.667	551	84.077	14.886	7.14	3.037	1.741
MgS	2630	0.995	496	110.88	44.545	4.68	9.288	2.144
MgSe	3064	2.810	483	683.66	218.98	4.02	18.84	2.270
Li	5249	0.608	454	35.177	49.514	2.35	33.73	1.977
Na	6650	0.315	445	34.324	21.219	1.85	35.37	1.579
Mg	6437	5.437	446	1268.7	1297.2	1.91	121.2	2.326

Journal Name RSCPublishing

ARTICLE

Table 2. Spectroscopic and covalency properties of the overlap charge density for alkali halide, alkali-earth chalcogenide and alkali diatomic molecules. Absorption wavelength λ_0 (nm) and its respective oscillator strength, f, Scattered λ_S photon wavelength (nm) and its respective scattering (Raman) cross-section σ_{Raman} (10^{-26} cm^2). Electron energy-loss cross-section σ_{Loss} (10^{-22} cm^2). Overlap charge characteristic energy E_p (eV). Overlap polarizability α_{op} (Å^3) and ionic specific valence υ.

Diatomic	λ_0	f	λ_S	σ_{Raman}	σ_{Loss}	E_p	α_{op}	υ
NaF	830	0.006	840	0.0012	0.0001	14.83	0.154	2.614
NaCl	1002	0.006	715	0.0033	0.0002	12.28	0.208	2.562
NaBr	935	0.003	754	0.0009	0.0000	13.17	0.131	2.577
CaO	1058	0.035	689	0.0021	0.0035	11.63	0.842	5.442
CaS	2237	0.539	513	0.5661	0.3232	5.50	10.58	5.654
CaSe	2590	0.746	498	1.0294	0.5909	4.75	16.19	5.758
MgO	2372	1.512	507	0.6158	1.8961	5.19	23.47	6.870
MgS	3592	3.455	472	3.7339	8.7298	3.43	71.63	6.993
MgSe	4536	6.546	460	9.6982	27.6603	2.71	151.3	7.289
LiLi	4713	0.598	458	53.1470	0.4022	2.61	25.00	1.651
NaNa	5191	0.485	454	76.4139	0.2956	2.37	24.94	1.489
MgMg	16151	0.028	429	0.0012	0.0001	0.76	24.73	0.167

Accordingly, the force constants of the diatomics follow this trend, whereas the solid-state systems follow a reverse trend. Indeed, this is observed in Table 2 that presents the results for the diatomics related to the solid-state systems (Table 1). Noteworthy that the overlap between the valence atomic orbitals of the species A–B in the chemical bond is strongly affected by the crystalline environment. For instance, the overlap in a chemical bond in the solid CaX (X = O, S, Se in Table S2) is larger than the overlap in the same bonds in the diatomic (Table S3), despite the bond distance in the diatomic being shorter than in the crystalline environment. In addition, the force constant in the isolated diatomic species is larger than the related bond in the solid-state, except for MgMg. The excitation energies related to the bonds in crystalline environments are larger than the isolated diatomic for all systems, except the metallic ones (Li, Na, Mg). These results and comparisons show the strong effects and relevance of the crystalline environment upon the parameters (R, ρ, k, $\Delta\varepsilon$) of the chemical bonds.

The calculated spectroscopic properties associated to the charge density in the overlap region of a chemical bond for NaY (Y = F, Cl, Br), MX (M = Ca, Mg and X = O, S, Se) and Li, Na, and Mg solids are presented in Table 1 and for their respective diatomic species are shown in Table 2. For some solid-state systems and diatomics, these properties have already been calculated and reported using different embedding scheme and computational methods. For the alkali-earth chalcogenides, a similar trend observed for the diatomic molecules is also present in the crystals, namely, the increase of the absorption wavelengths and the Raman scattering cross-sections with the increase in covalency.[14] Indeed, for these systems, the results reported in Tables 1 and 2 suggest that the calculated oscillator strengths (0.002 – 5.5) and Raman cross-sections (1×10^{-26} – 16×10^{-25} cm^2) are quite large, being greater than the range of scattering cross-sections ($\sim10^{-30}$ cm^2 per molecule) in conventional Raman scattering in different type of materials[28–32] thus, suitable for measurements even with a low sensitive apparatus. The higher values of scattering cross-sections was obtained for systems that present large overlap polatizability. Notice that these values are larger for the alkali-earth chalcogenides (solids or diatomics) than those obtained for the alkali halides (oscillator strengths in range of 0.002–0.006 and Raman cross-sections in range of 0.001×10^{-26} – 0.02×10^{-26} cm^2),[14] which indicate that more covalent chemical bonds lead to larger absorption or scattering. In addition, the calculated electron-energy cross-sections are in the same range of usual experimental values (10^{-22} – 10^{-23} cm^2)[33] and present similar trends observed for the Raman scattering with respect the covalency. However, the electron-energy cross-sections are much less sensitive to the covalency than the Raman scattering, but the energy loss cross-sections for the alkali-earth chalcogenides are very higher (three orders of magnitude) when compared with the values obtained for the alkali halides (crystals or diatomics).[14]

An interesting relationship between the ionic specific valence (υ) quantities and the absolute value of the sum of the Mulliken electronegativities $|\chi_A + \chi_B|$ was observed as depicted in Figure 4. Indeed, the sum of the atomic electronegativities is an index of the compactness of the valence orbitals of the atoms in the chemical bond A–B and have already been related to some chemical bond concepts such as the charge-shift resonance energy.[34] On the other hand, the ionic specific valence (υ)

quantifies the shared charge in bond A–B. In this sense, it is expected that the lower values of $|\chi_A + \chi_B|$ would give larger values of υ, given that less compact valence orbitals in atoms A and B may be more favorable to the sharing of electrons. This trend in observed at Figure 4 for fixed alkaline or alkaline-earth in series: NaF > NaCl > NaBr; CaO > CaS > CaSe; and MgO > MgS > MgSe. Thus, the results regarding the ionic specific valence corroborate our previews discussions[8] about the relations between this quantity and the meaning of the electronegativity in a chemical bond.

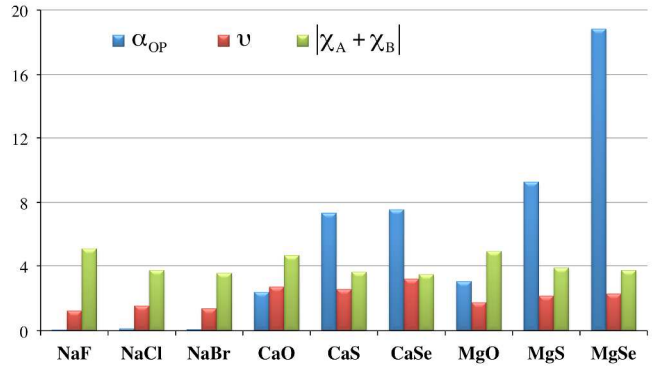

Figure 4. Calculated ionic specific valence (υ), sum of electronegativity $|\chi_A + \chi_B|$, and overlap polarizability α_{OP} (Å^3) for the alkali-earth chalcogenides and alkali-earth metals obtained with the Frozen Density Embedding approach for solid-state systems.

In Figure 4, the variation of $|\chi_A + \chi_B|$ for different systems is quite evident with respect to the α_{OP} for the same alkaline or alkaline-earth series: NaF > NaCl > NaBr; CaO > CaS > CaSe; and MgO > MgS > MgSe. This trend may be a consequence of the fact that α_{OP} quantity represents the polarization capacity of the valence overlap region between the atoms in the bond A–B. In this sense, a more compact valence (high value of $|\chi_A + \chi_B|$) should result in a less polarizable shared charge density and, consequently, small values of α_{OP}.

Alkali-earth sulfides and selenides presented very large overlap polarizability. These results may be interpreted by the atomic electronegativity and polarizability. For instance, the oxygen atom has a very large electronegativity (χ_O = 3.61), but a small polarizability (α_O = 0.8 Å^3), whereas the sulfur atom, compared to oxygen, has a smaller electronegativity (χ_S = 2.59) and a large polarizability (α_S = 2.9 Å^3), while the selenium atom has the smaller electronegativity (χ_{Se} = 2.43) and the greatest polarizability (α_{Se} = 3.77 Å^3) of the series O, S, Se (all atomic polarizabilities were obtained from the literature[35]). Thus, in the series O, S, Se, the oxygen atom is less prone to share its electrons because its electronegativity is the largest and its atomic polarizability is the smallest. Thus, the electron sharing propensity for this series increases in the order O > S > Se. In addition, because sulfur and selenium atoms have larger polarizabilities, it is expected that they should be more polarized upon the formation of a chemical bond compared to the oxygen atom. As a consequence, a chemical bond formed by more polarizable species and that exhibits more shared electronic density will present a more polarizable overlap region (larger α_{OP}), which is observed in Figure 4.

The same analogy may be employed for the alkali-earth metals, where χ_{Li} = 0.91 and α_{Li} = 24.3 Å^3; χ_{Na} = 0.86 and α_{Na} = 24.1 Å^3, which shows that the lithium and sodium atomic polarizabilities are practically the same, so the larger electronegativity of lithium suggests that this element would form less covalent bonds than sodium. We may then infer that the Li–Li chemical bond would share less charge density than a Na–Na bond in solid metals. Indeed, this trend may be observed from the overlap polarizability values in Table 1. For the chalcogenide series, the selenide compounds present the more favorable balance between the atomic electronegativity and polarizability, which makes the shared electron density in the overlap region more polarizable. This rationalization fails if only the atomic electronegativies (χ_X) or polarizabities (α_X) were employed, thus indicating that the combination of the ionic specific valence and the overlap polarizability becomes an interesting descriptor to qualify and quantify the shared electron density and its polarizability in a chemical bond. In fact, the balance between the atomic quantities χ_X and α_X are implicitly taken into accounted within the framework developed for the overlap region of a chemical bond.

The comparisons between the values presented in Tables 1 and 2 can provide qualitative and quantitative information about the effects of the crystalline environment on the overlap properties of a chemical bond. For instance, it is observed a general trend in the variation of α_{OP} in respect to the type of material. The α_{OP} of bonds in diatomics are larger than those α_{OP} of bonds in solids, where the crystalline environment was taken into account by frozen densities, when the system is dominated by an ionic character (Figures 5a, 5b and 5c). In contrast, for the homonuclear/metallic systems (LiLi, NaNa and MgMg) the α_{OP} is larger in the solid-state than in the isolated species. These results showed that the bond overlap charges are less polarizable (smaller α_{OP}) in the solid-state for dominantly ionic behavior as determined by the Pauling electronegativity differences, indicating that the chemical bond becomes less covalent in solids than in diatomics. Furthermore, this trend becomes even more evident for the ionic specific valence quantities, as can be observed Figure 5e.

Journal Name RSCPublishing

ARTICLE

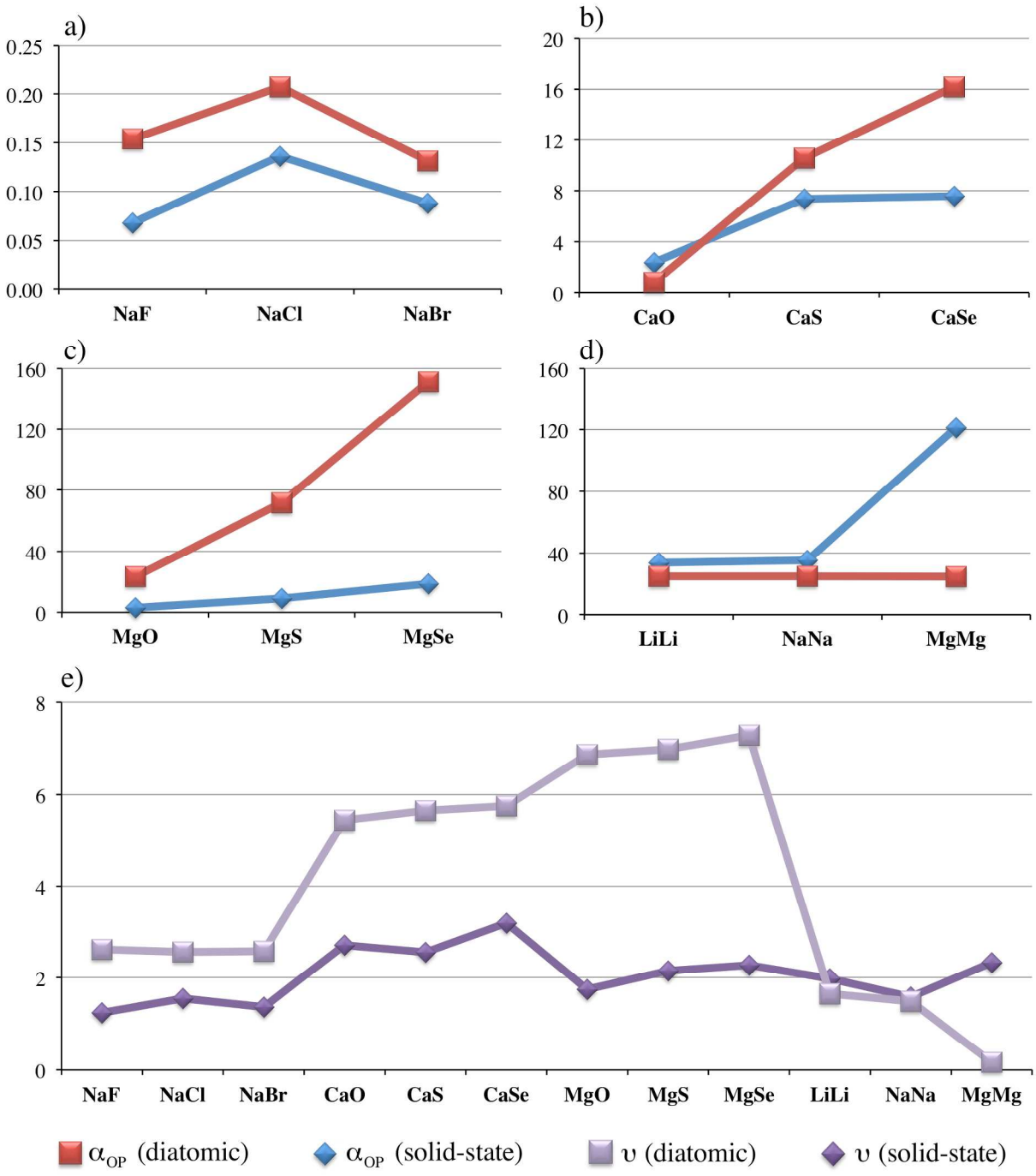

Figure 5. Calculated overlap polarizability α_{OP} (Å^3) and ionic specific valence υ for chemical bonds in alkali halides, alkali-earth chalcogenides, alkali and alkali-earth metals in isolated diatomics and in solid-state obtained with the Frozen Density Embedding approach.

The closeness of the characteristic energies (E_p) associated to the overlap density of chemical bonds in crystalline systems with some structures or peaks that appear in solid-state optical properties has already been pointed out[14] and shall be further

elaborated. Indeed, several of these optical property data show peaks or structures that were either ambiguously assigned or simply not assigned to any known behavior. The results presented in Tables 1 and 2 indicate that the spectroscopic properties of the polarizability of the electron density in the overlap region of a chemical bond could be measured in the 1–20 eV spectral region, where inter- and intra-band transitions, excitons, surface plasmons and the so-called zone boundary collective state (ZBCS) are observed. As pointed out previously,[14] the calculated overlap characteristic energies obtained for some alkali halides are close to the experimentally observed bands usually assigned as excitons. These results were corroborated by the embedding scheme proposed in this contribution and a similar behavior was observed for the alkali-earth chalcogenides. Indeed, several structures and shoulders that are arbitrarily assigned as excitons or surface plasmon because they are not present in any theoretical predictions of band structure calculations[36–38] and have transition energies smaller than the energy band gap. However, these features in the spectra are within the range of calculated spectroscopic properties of the charge density in the overlap region as summarized in Table 3.

Table 3. Characteristic energies of the overlap density, E_p (eV), and experimental, E_{exp} (eV), structures or shoulders with ambiguous or no assignments. ZBCS = zone boundary collective state.

Crystal	E_p	E_{exp}	Assignment	Type of measure
CaO	7.78	7	Exciton effect[36]	EELF
CaS	4.95	5	Exciton effect[36]	EELF
CaSe	5.54	--		
MgO	7.14	*ca.* 5	Not assigned[38]	
		6.2	Surface transition[38]	
		7.2	Excitonic absorption[37]	EELF; reflectivity
MgS	4.68	--	--	--
MgSe	4.02	--	--	--
Li	2.35	3.5–4.5	ZBCS[39,40]	EELF
Na	1.85	1.25–2.2	ZBCS[39]	Optical absorption
Mg	1.91	4.6	Not assigned[40]	Optical absorption

Noteworthy that the model is robust to provide consistent results even for homonuclear diatomics and alkali and alkali-earth metals. Regarding the experimental spectral data, they show anomalous features in spectral regions below the known interband transitions.[39–41] For the Li and Na metals, these peaks have been associated to a zone boundary collective state (ZBCS).[39,40] Indeed, quite some time ago, it was suggested[39] that in these cases, because the electrons are embedded into a periodic lattice, the electron energies are strongly perturbed near the zone boundary and the minimum photon energy needed to excite an electron from the Fermi surface to just above the energy gap at the zone boundary is close to the energy range of the anomalous effects found in these alkali-metals. By expressing the optical absorption as linear combinations of the self-consistent Hartree response functions[39] and applying it to the one reciprocal-lattice vector model, it was suggested that the low-energy peaks (below the interband transitions) should be associated with these Brillouin-zone boundaries effects. However, the characteristic energies of the overlap density in the chemical bond of alkali-metal systems are very close to these experimental anomalous peaks in the 2–4 eV spectral range. These agreements do reinforce the proposal that these effects are connected to the local oscillation of the confined overlap electron density in the chemical bond. At this point, we are not claiming a direct equivalence between the overlap density characteristic energy and the ZBCS effects, but we do believe that they are connected at least by their localized nature. In particular, the Li experimental results[41] have an interesting relation with the overlap density given that the EELF plasmon at 4.0 eV, assigned to ZBCS effects, have anisotropies in the momentum symmetry directions [100], [110] and [111], where a higher momentum transfer occurs in the [110] direction. This anisotropic behavior may be associated with the anisotropic character of the chemical bond, where for a diatomic homonuclear bond one must have two non-equivalent overlap polarizabilities (parallel and perpendicular to the internuclear axis) related with the directionality of the chemical bond. However, it must be emphasized that the current approach to determine the overlap polarizabilities of chemical bonds does not allow this kind of analysis directly. In fact, an extension of the current theoretical and computational approach to treat the anisotropy of overlap polarizabilities is one of the main perspective of this work.

Conclusions

It was shown that the Frozen Density Embedding approach is efficient and consistent to mimic the crystalline effects on the localized properties of chemical bonds. Noteworthy that consistent results were obtained using an appropriate computational protocol that involved a balanced description of the frozen and self-consistent cluster sizes. Also, allowing for the rearrangement of the density within the fragments self-consistently due to their mutual interactions is very important to achieve converged properties. The results showed that in solids with ionic character, the bond overlap charges are less polarizable than in the isolated diatomics, which according to the relationship between the overlap polarizability and covalency, suggest that the chemical bond becomes less covalent in the solid-state than in the isolated diatomic. The calculated overlap electron density characteristic energies for some solid-state systems such as alkali halides, alkali-earth chalcogenides, alkali and alkali-earth metals, are quite close to the experimental transition energies ambiguously assigned as excitons or ZBCS effects. Therefore, the spectral properties of the confined overlap density could be an alternative assignment to these observed features in the 1–20 eV energy range. Despite the approximations employed in the calculations of the properties (characteristic energy, oscillator strength, cross-section, polarizability) of the overlap charge density confined in a chemical bond, the present treatment provide energies that coincide with several experimental transitions and the trends may be consistently interpreted by combining the polarizability

and the ionic specific valence quantities. Considering the wide range of bonding situations and the consistency of the results obtained for these systems, the model is quite reliable regarding its accuracy, robustness, chemical and physical soundness as well as its importance as a probe to the covalency of molecules and materials.

Acknowledgements

The authors are grateful for the financial support from the Brazilian Agencies CNPq, CAPES and FINEP, from the State Agency FACEPE, from RENAMI and inct-INAMI Brazilian Scientific Programs, from PRONEX/FACEPE/CNPq (APQ-0859-1.06/08) and PNPD-CAPES/FACEPE (APQ-0397-1.06/12) Programs.

Notes and references

Departamento de Química Fundamental, Universidade Federal de Pernambuco, 50740-540, Recife-PE, Brazil.

Electronic Supplementary Information (ESI) available: [Detailed expressions for the overlap integrals and tables with calculated values of underlying properties of the overlap charge density model]. See DOI: 10.1039/b000000x/

1 G. N. Lewis, *J. Am. Chem. Soc.*, 1916, **38**, 762.
2 I. Langmuir, *J. Am. Chem. Soc.*, 1919, **41**, 868.
3 W. Heitler, F. London, *Zeitschrift für Physik*, 1927, **4**, 455 in H. Hettema, *Quantum Chemistry: Classic Scientific Papers* (World Scientific, Singapore 2000).
4 G. B. Bacskay, S. Nordholm, *J. Phys. Chem. A*, 2013, **117**, 7946.
5 L. Pauling, *J. Am. Chem. Soc.*, 1931, **53**, 1367.
6 C. A. Coulson, L. B. Redei, D. Stocker, *Proc. R. Soc. Lond. A,* 1962, **270**, 357.
7 J. C. Phillips, *Rev. Mod. Phys.,* 1970, **42**, 317.
8 O. L. Malta, H. J. Batista, L. D. Carlos, *Chem. Phys.,* 2002 **21**, 282.
9 L. D. Carlos, O. L. Malta, R. Q. Albuquerque, *Chem. Phys. Lett.,* 2005 **415**, 238.
10 O. L. Malta, *Chem. Phys. Lett.,* 1982, **88**, 353.
11 R. Q. Albuquerque, O. L. Malta In *NATO Science Series II: Mathematics, Physics and Chemistry*, J. C. Krupa, N. A. Kulagin, Eds, Kluwer Academic Publishers: Dordrecht, The Netherlands, 2003, **126**, 163.
12 O. L. Malta, *Chem. Phys. Lett.,* 2005, **406**, 192.
13 O. L. Malta, R. T. Moura Jr., R. L. Longo, *J. Braz. Chem. Soc.* 2010, **21**, 476.
14 R. T. Moura Jr., O. L. Malta, R. L. Longo, *Int. J. Quantum Chem.,* 2011, **111**, 1626.
15 G. P. Barnett, M. C. Pires Costa, R. Ferreira, *Chem. Phys. Lett*., 1974, **25**, 351.
16 V. Kondratyev, *The Structure of Atoms and Molecules, 2nd ed.* (Mir, Moscow) 1967, 445.
17 J. D. Jackson, *Classical Electrodynamics, 2nd ed.* (John Wiley & Sons Inc., New York) 1975, 284-296.
18 T. A. Wesolowski, A. Warshel, *J. Phys. Chem.,* 1993, **97**, 8050.
19 G. te Velde, F. M. Bickelhaupt, S. J. A. van Gisbergen, C. Fonseca Guerra, E. J. Baerends, J. G. Snijders, T. Ziegler, *J. Comp. Chem*., 2001, **22**, 931.
20 C. R. Jacob, J. Neugebauer, L. Visscher, *J. Comp. Chem.,* 2007, **29**, 1011.
21 J. Neugebauer, C. R. Jacob, T. A. Wesolowski, E. J. Baerends, *J. Phys. Chem. A*, 2005, **109**, 7805.
22 T. A. Wesolowski, *J. Phys. Chem.,* 1997, **106**, 8516.
23 A. Lembarki, H. Chermette, *Phys. Rev. A,* 1994, **50**, 5328.
24 W. H. Press, S. A. Teukolsky, W. T. Vetterling, B. P. Flannery, *Numerical Recipes in C - The Art of Scientific Computing 2nd ed.* (Cambridge University Press, Cambridge), 1992.
25 T. A. Wesolowski, J. Weber, *Chem. Phys. Lett.,* 1996 **248**, 71.
26 Y. A. Bernard, M. Dulak, J. W. Kaminski, T. A. Wesolowski, *J. Phys. A*, 2008, **41**, 55302.
27 W. A. Yeranos, J. D. Graham, *Spectrochim. Acta A*, 1967, **23**, 732.
28 R. L. Aggarwal, L. W. Farrar, S. K. Saikin, X. Andrade, A. Aspuru-Guzik, D. L. Polla, *Solid State Commun.*, 2012, **152**, 204.
29 R. L. Aggarwal, L. W. Farrar, S. K. Saikin, A. Aspuru-Guzik, M. Stopa, D. L. Polla, *Solid State Commun.*, 2011, **151**, 553.
30 W. F. Adolfson, R. G. Schlecht, J. B. Morton, *Appl. Phys.*, 1977, **14**, 49.
31 L. Li, T. Hutter, A. S. Finnemore, F. M. Huang, J. J. Baumberg, S. R. Elliott, U. Steiner, S. Mahajan, *Nano Lett.*, 2012, **12**, 4242.
32 S. Nie, S. R. Emory, *Science*, 1997, **275**, 1102.
33 R. Leapman In *Transmission Electron Energy Loss Spectrometry in Materials Science and the EELS Atlas, 2nd ed.* C. C. Ahn, Academic Publisher: WILEY-VCH, Wenheim 2004, 49-96.
34 S. Shaik, D. Danovich, B. Silvi, D. L. Lauvergnat, P. C. Hiberty, *Chem. Eur. J.*, 2005, **11**, 6358.
35 D. R. Lide (ed), *CRC Handbook of Chemistry and Physics, 90th Edition* (CRC Press/Taylor and Francis, Boca Raton, FL) 2010.
36 M. Dadsetani, H. Doosti, *Comp. Mater. Sci*., 2009, **45**, 315.
37 A. Schleife, C. Rödl, F. Fuchs, J. Furthmüller, F. Bechstedt, *Phys. Rev. B,* 2009, **80**, 035112.
38 V. E. Henrich, G. Dresselhaus, H. J. Zeiger, *Phys Rev B*, 1980, **22**, 4764.
39 K. Foot, J. J. Hopfield, *Phys. Rev.,* 1968, **173**, 635.
40 R. H. W. Graves, A. P. Lenham, *J. Opt. Soc. Am.* 1968, **58**, 884.
41 A. Rodriguez-Prieto, V. M. Silkin, A. Bergara, P. M. Echenique, *New. J. Phys.,* 2008, **10**, 053035.